Ring-vortex solitons and their stabilities in microcavity polariton condensates

Szu-Cheng Cheng[1], Shih-Da Jheng[1] and Ting-Wei Chen[2]

[1] Department of Optoelectric Physics, Chinese Culture University, Taipei 11114, Taiwan, R. O. C.
[2] Department of Electrophysics, National Chiayi University, Chiayi city 60004, Taiwan, R. O. C.

E-mail: twchen@mail.ncyu.edu.tw

Abstract

A ring-vortex soliton (RVS) is unstable in a uniform microcavity polariton condensate (MPC). We propose a method for generating a stable RVS in an MPC subjected to a ring-shaped defect potential. The density distribution of a RVS with a pump strength is obtained numerically for a given defect size and strength. Then we discover two types of RVSs: soliton with a dark ring and soliton with a gray ring. And the stabilities of RVSs are dependent on the pump and defect strength.

Keywords: exciton-polariton, vortex, soliton

(Some figures may appear in colour only in the online journal)

1. Introduction

Vortices are relevant in many areas of science, including particle physics [1–3], superfluids [4], condensed matter systems [5], ultracold atomic gases [6] and microcavity polaritons [7, 8]. They are characterized by the winding of a phase around a point known as the vortex core whose density is zero. Because the total phase change for a complete loop must be an integer multiple of 2π, a vortex is a state with quantized orbital angular momentum (OAM). Vortices have been intensively studied in classical systems including optical vortex beams [9] and lasers [10]. They are also the characteristic property of condensed-phase systems such as atomic Bose–Einstein condensates (BECs), liquid helium, and superconductors [11].

A ring-vortex soliton (RVS) is one of the most fascinating and universal structures in fluids of various natures. RVSs have been the subject of numerous studies on classical fluid mechanics [12], lasers and nonlinear optics [13–17]. In bulk optical media, toroidal dissipative solitons with an inner phase field in the form of rotating spirals have been studied using the complex Ginzburg–Landau equation with cubic-quintic nonlinearity [18]. Stable toroidal dissipative solitons could easily self-trap from pulses carrying orbital angular momentum. With respect to quantum fluids and degenerate gases, considerable efforts have been made to identify multidimensional solitons with vorticity [19–21]. RVSs with a

closed-loop core occupy a special place among other nonlinear excitations. RVSs play a crucial role in quantum turbulence and the decay of superflow [22]. Several experimental schemes for creating RVSs in BECs based on dynamical instabilities of collective excitations [23] or condensate collisions [24, 25] have been successfully tested. However, to meet the requirements of atomic BECs, an extremely low temperature is necessary to study the properties of the RVS. In contrast to atomic BECs, RVSs are easier to create in a polariton condensate because polariton BECs have been observed during experiments conducted at room temperature.

Polariton condensates in microcavities have been the topic of intensive research over the past two decades because of their progress towards a new generation of ultralow threshold lasers, ultrafast optical amplifiers, and room temperature switches [26]. Polaritons are bosonic quasiparticles that arise from strong exciton–photon coupling in semiconductor microcavities. Characteristic bosonic phenomena, such as stimulated scattering [27] and polariton condensation have been reported [28–31]. However, the polaritonic system is intrinsically out-of-equilibrium, meaning that continuous pumping is required to balance the fast polariton decay and sustain a steady-state solution [32–35]. The steady-state solution is characterized by a supercurrent that drives polaritons from gain-dominant to loss-dominated regions. In a nonresonantly pumped microcavity, polaritons from reservoir

turn into condensed polaritons and spontaneously evolve into vortices [36, 37] or vortex lattices [34] without stirring or rotating. The dynamics and properties of the polaritonic vortices have attracted intensive investigation in these two decades [38–41].

In this study, we propose a method for generating an RVS in a microcavity polariton condensate (MPC) with a ring-type defect in the system. The RVS state of MPCs has been studied using the complex Gross–Pitaevskii equation (cGPE) coupled to the reservoir polaritons at high momenta [33] with polariton mass m and interaction strength g between the condensed polaritons. This mean-field model for nonequilibrium MPCs is a generic model for evaluating the effects from pumping, dissipation, defect potential, relaxation and interactions. Because of the nonequilibrium character of MPCs, the excitation frequency Ω is a complex value [33, 42] whose real part, $\mathrm{Re}(\Omega)$, and imaginary part, $\mathrm{Im}(\Omega)$, represent the excitation energy and decay or growth rate of the system, respectively. The stability of an RVS is justified by $\mathrm{Im}(\Omega)$, provided that $\mathrm{Im}(\Omega) < 0$.

2. Model

In semiconductor microcavities, a nonresonant excitation leads to photo-creation of electron-hole pairs, which quickly cool through the emission of phonons to create polaritons, which populate the lower polariton branch (LPB) at high $k_{//}$-values. Subsequent steps consist of polariton relaxation (mostly through polariton–polariton scattering) on the LPB towards the radiative states at the bottom of the LPB near $k_{//} = 0$. In a larger time frame, the *non-condensed* polaritons near $k_{//} = 0$ may either decay through radiative and non-radiative recombinations or replenish into the coherent *condensed* polaritons with slightly higher blue-shift energy equal to the repulsive nonlinear interaction energy [28]. Therefore, we treat the *non-condensed* polaritons as a reservoir and employ the dissipative cGPE for a condensate that is coupled to the reservoir. The system is uniformly pumped with a pump power P, which contributes to population of the reservoir polaritons near $k_{//} = 0$ during a short time frame. Let $\Psi(\vec{r}, t)$ and $n_R(\vec{r}, t)$ represent the MPC wave function and reservoir polariton density, respectively, the dynamics of the MPC and reservoir polaritons are then given by:

$$i\hbar \frac{\partial \Psi}{\partial t} = -\frac{\hbar^2}{2m}\nabla^2\Psi + V(\vec{r})\Psi$$
$$+ \frac{i}{2}\hbar\left[R(n_R) - \gamma\right]\Psi + g|\Psi|^2\Psi + 2\tilde{g}n_R\Psi, \quad (1)$$

$$\frac{\partial n_R}{\partial t} = P - \gamma_R n_R - R(n_R)|\Psi|^2, \quad (2)$$

where m is the polariton mass, $\hbar$ is the Planck constant. $V(\vec{r})$ is the defect potential of polaritons. $R(n_R)$ is the replenishment rate of the *condensed* polaritons from the *non-condensed* reservoir polaritons, γ describes the polariton decay rate due to of the imperfections of the cavity mirrors, γ_R is the decay

rate of reservoir polaritons, and g and $\tilde{g}$ ($\tilde{g} = 2g$ under the Hartree–Fock approximation) are the coupling constants of polariton–polariton interactions and condensate-reservoir interactions, respectively [33].

For nonequilibrium MPCs, we treat the polaritons at high momenta as a reservoir and employ the cGPE, using the condensed polaritons that couple to the reservoir polaritons with density $n_{\mathbf{R}}(\mathbf{r}, t)$, to describe the time evolution and probability amplitude function $\Psi(\mathbf{r}, t)$ of the condensate. In the cGPE, we add a defect potential with a ring-shaped form $V(\vec{r}) = V_0 e^{-(r-r_0)^2/a^2}$ to the equation to mimic a potential defect. Besides, a pumping term with power P that exceeds the threshold of P_{th} ($P > P_{th}$) is introduced into the rate equation of reservoir. By selecting the length, energy and time scales in units of $\lambda = \sqrt{\hbar^2\gamma\sigma/2mgP_{\mathrm{th}}}$, $\hbar\omega_0 = \hbar^2/2m\lambda^2$ and $\tau = 1/\omega_0$, respectively, in which $\sigma = 1/[1 - (4\gamma/\gamma_R)]$ is associated with the relative decay rate, we can rescale the wave function of the condensed polaritons as $\psi(\boldsymbol{\rho}, \tau) = \Psi(\mathbf{r}, t)/\sqrt{n_c}$ and the reservoir polariton density as $n(\boldsymbol{\rho}, \tau) = n_{\mathbf{R}}(\mathbf{r}, t)/n_R^{th}$. Here $n_c = |\Psi(\mathbf{r} \to \infty, \tau)|^2$ represents the steady-state condensate density far from the vortex core, and $n_R^{th} = P_{th}/\gamma_R$ is the reservoir density at the threshold pumping power P_{th} in the unit of decay rate of the reservoir polaritons γ_R. $\boldsymbol{\rho} = (\rho, \theta)$ with $\rho = r/\lambda$ being the dimensionless radial coordinate. After this rescaling, the condensate wave function $\psi(\boldsymbol{\rho}, \tau)$ and reservoir density $n(\boldsymbol{\rho}, \tau)$ satisfy the coupled differential equations as follows [37]

$$i\frac{\partial \psi}{\partial \tau} = -\nabla_\rho^2\psi + \tilde{V}\psi + \frac{i}{2}[\tilde{R}(n) - \tilde{\gamma}]\psi$$
$$+ \alpha\sigma|\psi|^2\psi + (\sigma - 1)n\psi, \quad (3)$$

$$\frac{\partial n}{\partial \tau} = \tilde{\gamma}_R(\alpha + 1 - n) - 4\tilde{R}(n)\left(\frac{\alpha\sigma}{\sigma - 1}\right)|\psi|^2. \quad (4)$$

Here the Laplacian operator associated with the dimensionless polar coordinate ρ is defined as $\nabla_\rho^2 \equiv \frac{1}{\rho}\frac{\partial}{\partial\rho}\left(\rho\frac{\partial}{\partial\rho}\right) + \frac{1}{\rho^2}\frac{\partial^2}{\partial\theta^2}$. The scaled defect potential $\tilde{V}(\rho) = V_1 e^{-(\rho-\rho_0)^2/a_1^2}$ had the dimensionless potential strength $V_1 = V_0/\hbar\omega_0$ and width $a_1 = a/\lambda$ positioned at a distance ρ_0 away from the center of the condensate. $\alpha = (P/P_{th}) - 1$ was the relative pumping intensity beyond the threshold. $\tilde{\gamma}_R/\tilde{\gamma} = 5$ are chosen based on previous literatures [33, 43]. The other notations indicated the following. $\tilde{R}(n) = R(n_{\vec{R}})/\omega_0$ is the dimensionless amplification rate describing the replenishment of the condensate state from the reservoir state through stimulated scattering; $\tilde{\gamma} = \gamma/\omega_0$ and $\tilde{\gamma}_R = \gamma_R/\omega_0$ are the decay rates of condensate and reservoir polaritons, respectively.

3. Steady-state ring-vortex solitons

The solutions of equations (3) and (4) with $\tilde{V}(\rho) \neq 0$ differ from those for the homogeneous MPC without defect potential. For a finite defect, the amplification rate $\tilde{R}(n)$ has spatial dependence rather than being uniform across the entire system. In such a steady state, fluxes that connect the regions of loss and gain constantly occur, leading to the possible
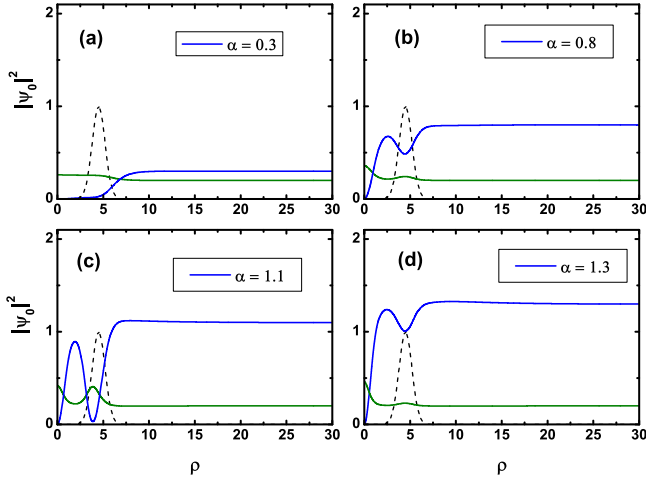
Figure 1. Radial density profiles of ring-vortex solitons (blue solid lines) and reservoirs (green solid lines): (a) $\alpha = 0.3$, (b) $\alpha = 0.8$, (c) $\alpha = 1.1$ and (d) $\alpha = 1.3$. Parameters: $V_1 = 1$, $a_1 = 1$, $\rho_0 = 4.5$, $\tilde{\gamma} = 1$, and $\tilde{\gamma}_R = 5$. The winding number of a vortex is $m_\ell = 1$. The Gaussian potentials are presented as black dashed lines for reference.

Figure 2. Density profiles of ring-vortex solitons (blue solid lines) and reservoirs (green solid lines): (a) $V_1 = 0$, (b) $V_1 = 0.5$, (c) $V_1 = 1$ and (d) $V_1 = 2$. Parameters: $\alpha = 1.1$, $a_1 = 1$, $\rho_0 = 4.5$, $\tilde{\gamma} = 1$, $\tilde{\gamma}_R = 5$. The winding number of a vortex is $m_\ell = 1$, and the Gaussian potentials are presented as black dashed lines for reference.

formation of a dynamically stable condensate. We assume that the amplification rate is a linear function of reservoir density (i.e. $\tilde{R}(n) = \tilde{\beta}n$, with $\tilde{\beta}$ being a constant). This is an accurate approximation for a weak pumping regime. The steady state of the system under uniform pumping could therefore be obtained by substituting $\psi(\rho, \theta) = \psi_0(\rho)e^{im_\ell\theta - i\tilde{\mu}\tau}$ into equations (3) and (4), where m_ℓ is the winding number of a vortex and $\tilde{\mu} = \mu/\hbar\omega_0$ is the dimensionless chemical potential of the system. In the limit $\rho \to \pm\infty$, $\psi_0(\rho) \to 1$ and $n_0 \to 1$, we discover that $\tilde{\beta} = \tilde{\gamma}$ under the steady state of the system and the chemical potential of the system is given by $\tilde{\mu} = \alpha\sigma + (\sigma - 1)$. Applying $\tilde{R}(n) = \tilde{\gamma}n$ and $\tilde{\mu}$ to the steady states of equations (3) and (4), we obtain

$$\frac{d^2\psi_0}{d\rho^2} + \frac{1}{\rho}\frac{d\psi_0}{d\rho} - \frac{m_\ell^2}{\rho^2}\psi_0 - V(x)\psi_0 + \alpha\sigma(1 - |\psi_0|^2)\psi_0$$
$$- (\sigma - 1)(n_0 - 1)\psi_0 - \frac{i\tilde{\gamma}}{2}(n_0 - 1)\psi_0 = 0, \quad (5)$$

where $n_0 = \frac{(\alpha + 1)}{(\alpha|\psi_0|^2 + 1)}$. We can solve equation (5) numerically by using the Newton–Raphson method. In the following discussions, we will see that the dips in the vortex core and dark ring contain some reservoir polaritons in the background, which is consistent with experimentally observed vortex density patterns [44].

We calculate the density distributions of the steady states of polariton condensates for various uniform pumps under the defect potential of constant width ($a_1 = 1$) and strength ($V_1 = 1$) in figure 1. For the low pump strength displayed in figure 1(a), a vortex with $m_\ell = 1$ can be observed in a uniform MPC background at $\rho = 0$. With increased pump strength crossing the first critical value (~0.53 for $V_1 = 1$) to a moderate value ($\alpha = 0.8$), as presented in figure 1(b), a bright part loops away from the vortex core and back on itself to form a gray-ring part accompanied with the outer uniform MPC background. It is a solution with all three characteristics: core and ring, separated by a hump. Therefore, the two-
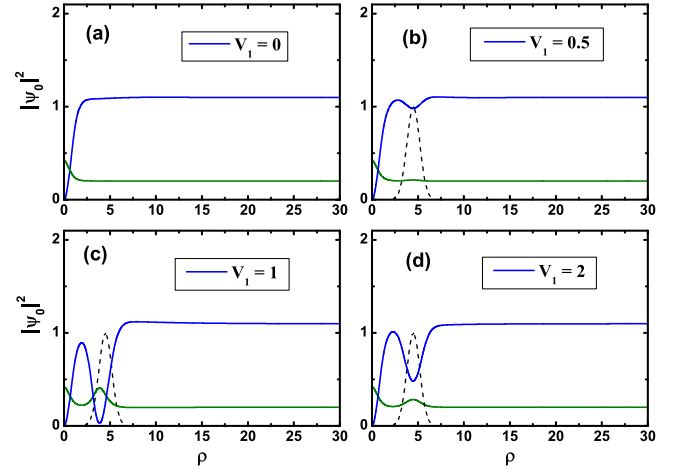
dimensional MPC has the density profile of an RVS with a concentric gray ring around its core. As the pump strength is increased crossing a second critical value (~1.06 for $V_1 = 1$), the reservoir polariton density is increased (peak value from 0.24 in figure 1(b) to 0.41 in figure 1(c) around $\rho \sim 4.5$) so that the gray ring becomes dark since the repulsive force from reservoir polaritons on the condensed polaritons is increased (see figure 1(c)). The condensed polariton density in the dark ring region centered around $\rho \sim 4.5$ is almost negligible ($|\psi_0|^2 \sim 0.02$). When the pump strength is increased higher than a third critical value (~1.23 for $V_1 = 1$), the reservoir polariton density starts to decrease dramatically compared with that of figure 1(c), piling up some condensed polaritons back into the dip around $\rho \sim 4.5$, creating the gray ring again as presented in figure 1(d).

Figure 2 displays the density distributions of $\alpha = 1.1$ with varying defect potential V_1. Figure 2(a) demonstrates that the RVS solutions do not exist in the absence of defect potential. This indicates that the bright ring part of the RVS is artificially created by the defect potential. It is not an intrinsic solution of the nonequilibrium polariton system without the defect potential. Moreover, the defect potential here not only creates the RVS but plays the role of stabilizing the RVSs under certain pump strengths and defect conditions.

4. Stabilities of ring-vortex solitons

Having determined the density profiles of the steady states of RVSs, we investigate the excitations and stability of an RVS. We consider the small fluctuations $\delta\psi$ and δn acting on the steady state ψ_0 and n_0 of the system that has an RVS with an angular momentum characterized by the quantum number $m_\ell = 1$. Though the steady-state solution is rotationally invariant, we still assume the excitation being a general non-

symmetrized excitations:

$$\psi(\rho, \theta) = e^{-i\mu\tau}e^{im_\ell\theta}[\psi_0(\rho) + u(\rho, \theta)e^{-i\Omega\tau} + v^*(\rho, \theta)e^{i\Omega\tau}], \quad (6)$$

$$n(\rho, \theta) = n_0 + w(\rho, \theta)e^{-i\Omega\tau} + w^*(\rho, \theta)e^{i\Omega\tau}, \quad (7)$$

where u, v, w are the amplitudes of the excitation quasi-particles, and Ω is the index labeling the excitation frequency. The excitation frequency indicates the phase fluctuation of any of the small fluctuating components, which is the phase of the excited collective condensate state. For a none-equilibrium system such as the exciton–polaritons inside the microcavity, the excitation frequency is a complex number. By substituting $\psi(\rho, \theta)$ and $n(\rho, \theta)$ into equations (3) and (4) and linearizing them around the steady state, we obtain three coupled Bogoliubov equations [45] that could be used to study the excitations and stability of the system:

$$-\Delta_+ u + (A(\rho) - \mu)u + B(\rho)v + C(\rho)w = \Omega u, \quad (8)$$

$$\Delta_- v - (A^*(\rho) - \mu)v - B^*(\rho)u - C^*(\rho)w = \Omega v, \quad (9)$$

$$-iF^*(\rho)u - iF(\rho)v - iG(\rho)w = \Omega w, \quad (10)$$

where the operators $\Delta_\pm = (1/\rho)\partial/\partial\rho(\rho\partial/\partial\rho) + (1/\rho^2)(\partial^2/\partial\theta^2) \pm (2im_\ell/\rho^2)(\partial/\partial\theta) - m_\ell^2/\rho^2$, $A(\rho) = 2\alpha\sigma|\psi_0|^2 + V(\rho) + (\sigma - 1)n_0 + \frac{i\tilde{\gamma}}{2}(n_0 - 1)$, $B(\rho) = \alpha\sigma\psi_0^2$, $C(\rho) = [i\tilde{\gamma}/2 + (\sigma - 1)]\psi_0$, $F(\rho) = 4\tilde{\gamma}(\frac{\sigma}{\sigma-1})\alpha n_0\psi_0$ and $G(\rho) = 4\tilde{\gamma}(\frac{\sigma}{\sigma-1})[1 + \alpha\sigma|\psi_0|^2]$. Of the many excitation states, we are primarily interested in the branch with the lowest excitation frequency. The decay [Im $(\Omega) < 0$] and growth [Im $(\Omega) > 0$] behaviors of the excitation mode indicate the stability and instability of the steady state of the system, respectively.

By establishing a uniform pumping power scheme, we test the stability of the steady-state RVSs through the three coupled Bogoliubov equations (8)–(10). No stable RVS is observed in a uniform MPC. However, depending on the pump and defect potential strengths, the RVS could be stabilized by introducing a ring-shaped defect into an MPC. The excitation frequencies of the steady RVSs with respect to the angular momentum ℓ are displayed in figure 3 for the defect potential of constant width ($a_1 = 1$) and strength ($V_1 = 1$). The stability of an RVS is fulfilled if Im$(\Omega) < 0$, where Ω is the excitation frequency of the system. For the vortex under a low pump strength, as displayed in figure 1(a), we observe that the vortex is unstable as shown in figure 3(a). After increasing the pump strength to a moderate value as displayed in figure 1(b), the overall density grows up with a dip region caused by the repulsive force of the defect potential. However, the local increase of the reservoir polariton density around the center of defect is insufficient to fully deplete the condensed polaritons out of the dip. Thus the steady-state solution is a gray RVS. The stability analysis in figure 3(b) indicates that the RVS in MPCs can be stabilized with a defect potential that has suitable strengths and widths. Local accumulation of the reservoir density, which is related to both V_1 and α, should create an effective potential barrier that can repel the condensed polaritons around the dip [33]. Though a constant inward flow is directed into the dip [46], the
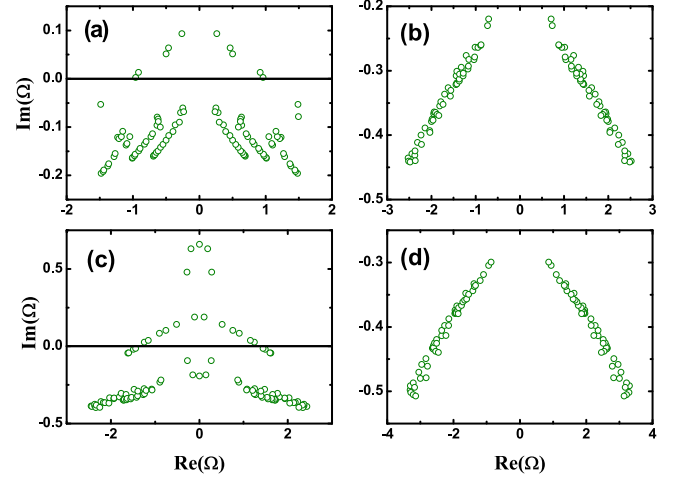

Figure 3. Bogoliubov excitation spectra for $V_1 = 1$ and $a_1 = 1$. (a) $\alpha = 0.3$; (b) $\alpha = 0.8$; (c) $\alpha = 1.1$; (d) $\alpha = 1.3$. The instabilities are revealed by the positive imaginary parts of the excitation eigen-energies.
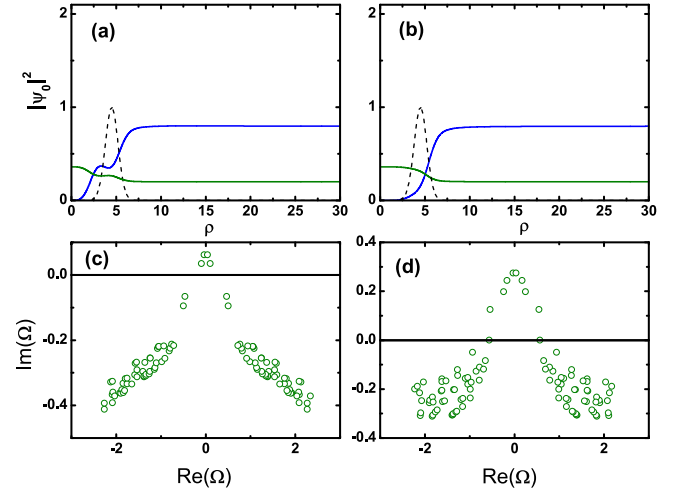

Figure 4. Radial density profiles and Bogoliubov excitation spectra of stable RVSs for higher topological charges at $\alpha = 0.8$. (a)–(c) $m_\ell = 2$; (b)–(d) $m_\ell = 3$. Parameters: $V_1 = 1$, $a_1 = 1$, $\rho_0 = 4.5$, $\tilde{\gamma} = 1$, and $\tilde{\gamma}_R = 5$.
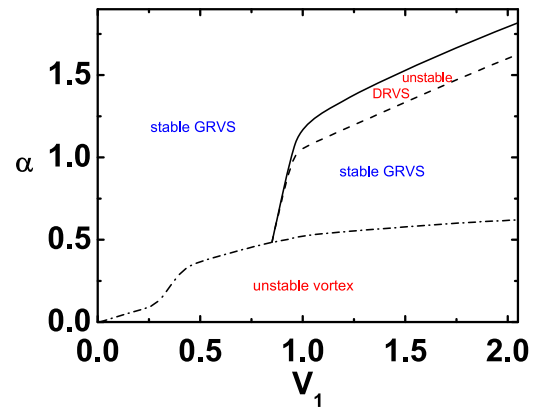

Figure 5. Phase diagram of ring-vortex solitons under a fixed defect width $a_1 = 1$. Abbreviations DRVS and GRVS represent the ring-vortex soliton with a dark ring and ring-vortex soliton with a gray ring, respectively.
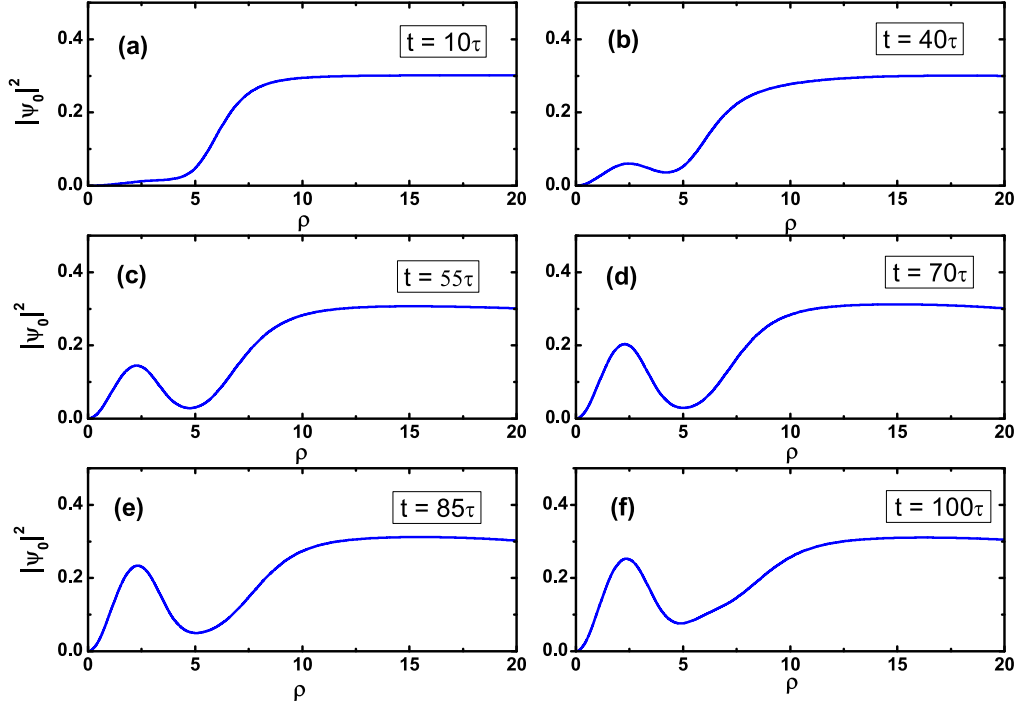
J. Phys. B: At. Mol. Opt. Phys. **53** (2020) 045401

S-C Cheng *et al*

Figure 6. Numerical simulations of the RVS for $\alpha = 0.3$ with simulated time interval of (a) $t = 10\tau$; (b) $t = 40\tau$; (c) $t = 55\tau$; (d) $t = 70\tau$; (e) $t = 85\tau$; (f) $t = 100\tau$. Parameters: $V_1 = 1$, $a_1 = 1$, $\rho_0 = 4.5$, $\tilde{\gamma} = 1$, and $\tilde{\gamma}_R = 5$. The winding number of a vortex is $m_\ell = 1$.
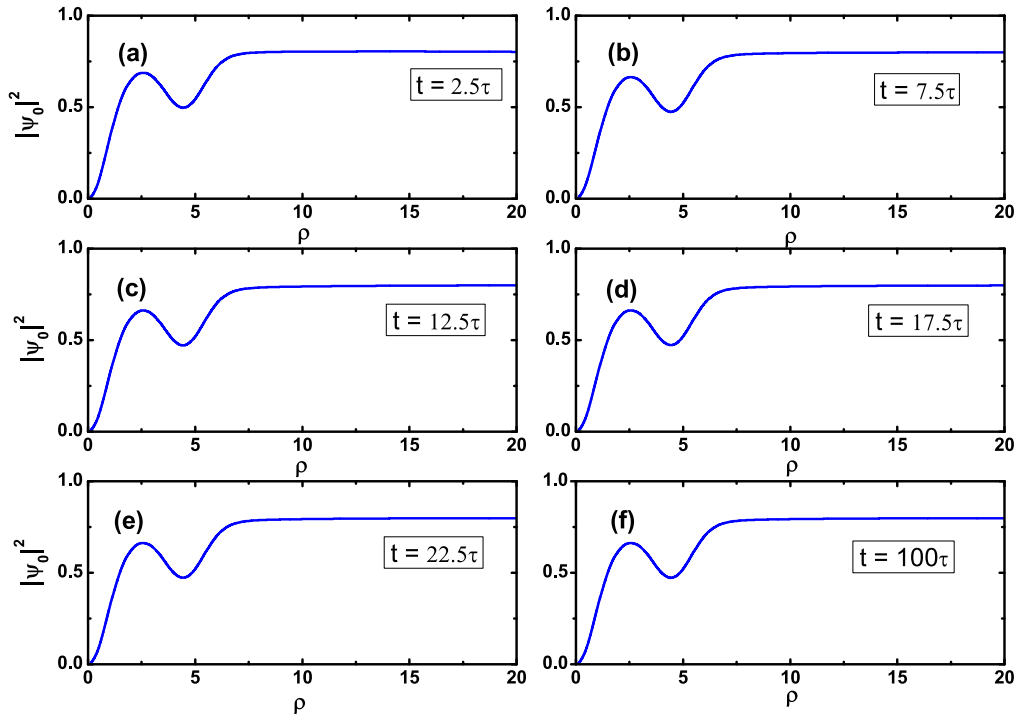

Figure 7. Numerical simulations of the RVS for $\alpha = 0.8$ with simulated time interval of (a) $t = 2.5\tau$; (b) $t = 7.5\tau$; (c) $t = 12.5\tau$; (d) $t = 17.5\tau$; (e) $t = 22.5\tau$; (f) $t = 100\tau$. Parameters: $V_1 = 1$, $a_1 = 1$, $\rho_0 = 4.5$, $\tilde{\gamma} = 1$, and $\tilde{\gamma}_R = 5$. The winding number of a vortex is $m_\ell = 1$.

repulsive force from the defect potential and reservoir's potential are still sufficient to prevent condensed polaritons from further flowing into the gray ring and sustain a steady-state density profile. Therefore, a stabilized RVS can occur in a nonequilibrium MPC with defects. Further increasing the pump strength to an even higher value as displayed in

figure 1(c), the reservoir polariton density inside the ring is increasing so that more condensed polaritons are depleted in the dip and the gray ring becomes dark (see figure 3(c)). However, the RVS with a dark ring (see figure 3(c)) is unstable and will eventually become an RVS with a gray ring (see time evolution in figure 8). The non-monotonic transition
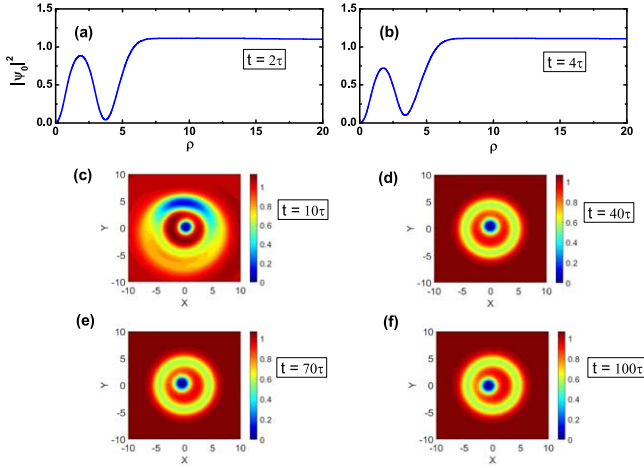
J. Phys. B: At. Mol. Opt. Phys. **53** (2020) 045401

S-C Cheng *et al*

Figure 8. Numerical simulations of the RVS for $\alpha = 1.1$ with simulated time interval of (a) $t = 2\tau$; (b) $t = 4\tau$; (c) $t = 10\tau$; (d) $t = 40\tau$; (e) $t = 70\tau$; (f) $t = 100\tau$. Parameters: $V_1 = 1$, $a_1 = 1$, $\rho_0 = 4.5$, $\tilde{\gamma} = 1$, and $\tilde{\gamma}_R = 5$. The winding number of a vortex is $m_\ell = 1$.
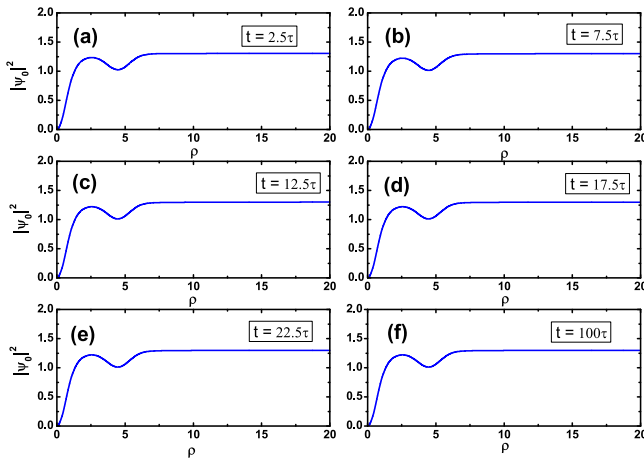

Figure 9. Numerical simulations of the RVS for $\alpha = 1.3$ with simulated time interval of (a) $t = 2.5\tau$; (b) $t = 7.5\tau$; (c) $t = 12.5\tau$; (d) $t = 17.5\tau$; (e) $t = 22.5\tau$; (f) $t = 100\tau$. Parameters: $V_1 = 1$, $a_1 = 1$, $\rho_0 = 4.5$, $\tilde{\gamma} = 1$, $\tilde{\gamma}_R = 5$. Here the winding number of a vortex is $m_\ell = 1$.

from figures 1(c) to (d) is due to the rapid decrease of the reservoir polariton density inside the dip of the ring. The depletion effect from decreased reservoir polaritons is overwhelmed by the replenishment of condensed polaritons due to increased pumping. Therefore, the RVS turns to a gray ring and it is unstable from the stability analysis (see figure 3(d)).

RVSs with higher topological charges, such as $m_\ell = 2, 3$, can not exist in the nonequilibrium polariton system. Examples of the instabilities of RVSs with higher m_ℓ are presented in figure 4. As displayed in figure 4, RVSs in an MPC could not be stabilized under a repulsive defect potential. Figure 5 presents the existence domains of RVSs in terms of the strength of the defect potential and pump strength under a constant defect width. The RVS with a gray ring is always stable. For a given low defect strength, the RVS with a gray ring can exist at a higher pump strength. When the defect strength increases, the RVS with a gray ring can exist at two

regimes of pump strength separated by a regime of unstable RVS with a dark ring.

5. Numerical simulations of the RVSs

We directly apply two-dimensional numerical simulations to confirm the phase diagram obtained in figure 5. We numerically solve the time evolution equations of equations (3) and (4). The steady states presented in figure 1 with an extra noise term are treated as the initial states of the time-evolving processes governed by equations (3) and (4) Modulus-Squared Boundary Conditions are applied [47] to deal with the converging function value at the boundary. The time intervals are successively increased and the corresponding numerical results are displayed separately in six sub-figures with time step equal to $0.000\,2\tau$. The numerical results for different states shown in figure 1 are presented in figures 6–9. The first case with $\alpha = 0.3$ and $V_1 = 1$ is an unstable vortex. Concentric ring soliton is not formed yet. The initial vortex profile evolves to a continuously-changing gray RVS (GRVS) and never returns to its steady-state structure (figure 6). Thus the vortex is not a steady-state solution. The second case with $\alpha = 0.8$ and $V_1 = 1$ is a stable gray RVS (GRVS). The initial profile does not evolve to another structure, it is stabilized quickly to a GRVS. We can see that the density profile does not change with time from the very beginning. The height of the bright part from the dynamical evolution is nearly the same as that from the steady-state prediction in figure 1 (see figure 7). The third case with $\alpha = 1.1$ and $V_1 = 1$ is an unstable dark RVS (DRVS). Its ring still remains dark from the initial time point to around $t = 2\tau$, then we observe its evolution to a GRVS within 2τ as shown from figures 8(a) to (b). The time evolution ended in a non-central-symmetrically rotating gray RVS. From figures 8(c) to (f), the core of the vortex is off-center and rotates around the center of the condensate slowly with time. The four panes of 2D density distribution at four distinct time moments are shown instead of 1D radial density profiles. We can see that the dark RVS is not a stable solution, it is continuously evolving. The fourth case with $\alpha = 1.3$ and $V_1 = 1$ is again a stable GRVS because its initial gray ring is sustained with time, as displayed in figure 9. Likewise, we observed that the height of the bright part from the dynamical evolution is the same as that from the steady-state prediction.

6. Conclusions

In summary, an RVS in a homogeneous microcavity polariton condensate without defect potential is unstable. RVSs can be created by adding a ring-shaped defect potential to the microcavity polariton condensate. We demonstrate that two types of RVSs exist, namely GRVSs and DRVSs. The GRVS is stable when the pump power and defect strength are within suitable values. However, the DRVS is unstable since the repulsive force from the reservoir polaritons are insufficient to

prevent condensed polaritons from further flowing into the dip region. Therefore the time evolution ended in GRVSs, and their steady-states are unstable.

Acknowledgments

ORCID iDs

Ting-Wei Chen https://orcid.org/0000-0003-1728-4946

References

[1] de Vega H J and Schaposnik F A 1976 *Phys. Rev. D* **14** 1100
[2] Kleihaus B, Kunz J and Shnir Y 2004 *Phys. Rev. D* **70** 065010
[3] Bruckmann F, Ilgenfritz E M, Martemyanov B and Zhang B 2010 *Phys. Rev. D* **81** 074501
[4] Sonin E B 1987 *Rev. Mod. Phys.* **59** 87
[5] Altshuler E and Johansen T H 2004 *Rev. Mod. Phys.* **76** 471
[6] Ramachandhran B, Opanchuk B, Liu X J, Pu H, Drummond P and Hu H 2012 *Phys. Rev. A* **85** 023606
[7] Lagoudakis K G, Ostatnický T, Kavokin A V, Rubo Y, André R and Deveaud-Plédran B 2009 *Science* **326** 974
[8] Nardin G, Grosso G, Leger Y, Pietka B, Morier-Genoud F and Deveaud-Plédran B 2011 *Nat. Phys.* **7** 635
[9] Allen L *et al* 1992 *Phys. Rev. A* **45** 8185
[10] Scheuer J and Orenstein M 1999 *Science* **285** 230
[11] Pitaevski L and Stringari S 2003 *Bose–Einstein Condensation* (Oxford: Oxford University Press)
[12] Saffman P G 1992 *Vortex Dynamics* (Cambridge: Cambridge University Press)
[13] Rosanov N N 2004 *Lect. Notes Phys.* **661** 101–130
[14] Rosanov N N, Fedorov S V and Shatsev A N 2005 *Phys. Rev. Lett.* **95** 053903
[15] Paulau P V, Gomila D, Colet P, Loiko N A, Rosanov N N, Ackemann T and Firth W J 2010 *Opt. Express* **18** 8859
[16] Jimenez J, Noblet Y, Paulau P V, Gomila D and Ackemann T 2013 *J. Opt.* **15** 044011
[17] Desyatnikov A S, Kivshar Y S and Torner L 2005 *Prog. Opt.* **47** 291–391
[18] Mihalache D, Mazilu D, Lederer F, Kartashov Y V, Crasovan L C, Torner L and Malomed B A 2006 *Phys. Rev. Lett.* **97** 073904
[19] Carr L D and Clark C W 2006 *Phys. Rev. A* **74** 043613
[20] Li J, Wang D S, Wu Z Y, Yu Y M and Liu W M 2012 *Phys. Rev. A* **86** 023628
[21] Yukalov V I, Novikov A N, Yukalova E P and Bagnato V S 2016 *J. Phys.: Conf. Ser.* **691** 012019
[22] Tsubota M, Kobayashi M and Takeuchi H 2013 *Phys. Rep.* **522** 191
[23] Anderson B P *et al* 2001 *Phys. Rev. Lett.* **86** 2926
[24] Ginsberg N S, Brand J and Hau L V 2005 *Phys. Rev. Lett.* **94** 040403
[25] Shomroni I, Lahoud E, Levy S and Steinhauer J 2009 *Nat. Phys.* **5** 193
[26] Deng H, Haug H and Yamamoto Y 2010 *Rev. Mod. Phys.* **82** 1489
[27] Stevenson R M *et al* 2000 *Phys. Rev. Lett.* **85** 3680
[28] Kasprzak J *et al* 2006 *Nature* **443** 409
[29] Balili R *et al* 2007 *Science* **316** 1007
[30] Deng H *et al* 2007 *Phys. Rev. Lett.* **99** 126403
[31] Amo A *et al* 2009 *Nature* **457** 291
[32] Marchetti F M, Szymańska M H, Tejedor C and Whittaker D M 2010 *Phys. Rev. Lett.* **105** 063902
[33] Wouters M and Carusotto I 2007 *Phys. Rev. Lett.* **99** 140402
[34] Keeling J and Berloff N G 2008 *Phys. Rev. Lett.* **100** 250401
[35] Borgh M O, Keeling J and Berloff N G 2010 *Phys. Rev. B* **81** 235302
[36] Lagoudakis K G, Wouters M, Richard M, Baas A, Carusotto I, André R, Dang L S and Deveaud-Plédran B 2008 *Nat. Phys.* **4** 706
[37] Chen T W, Chiang Y L, Cheng S C and Hsieh W F 2013 *Solid State Commun.* **165** 6
[38] Lagoudakis K G, Manni F, Pietka B, Wouters M, Liew T C H, Savona V, Kavokin A V, André R and Deveaud-Plédran B 2011 *Phys. Rev. Lett.* **106** 115301
[39] Fraser M D, Roumpos G and Yamamoto Y 2009 *New J. Phys.* **11** 113048
[40] Padhi B, Duboscq R, Niranjan A and Soni R K 2015 *Eur. Phys. J. B* **88** 116
[41] Dominici L Z *et al* 2018 *Nat. Commun.* **9** 1467
[42] Szymańska M H, Keeling J and Littlewood P B 2006 *Phys. Rev. Lett.* **96** 230602
[43] Gao T, Egorov O A, Estrecho E, Winkler K, Kamp M, Schneider C, Höfling S, Truscott A G and Ostrovskaya E A 2018 *Phys. Rev. Lett.* **121** 225302
[44] Krizhanovskii D N *et al* 2010 *Phys. Rev. Lett.* **104** 126402
[45] Bogoliubov N N 1947 *J. Phys. (USSR)* **11** 23
[46] Chen T W, Cheng S C and Hsieh W F 2013 *Phys. Rev. B* **88** 184502
[47] Caplan R M and Carretero-González R 2014 *SIAM J. Sci. Comput.* **36** A1–19